LIMNOLOGY and OCEANOGRAPHY



Limnol. Oceanogr. 67, 2022, 2265–2280 © 2022 Association for the Sciences of Limnology and Oceanography. doi: 10.1002/lno.12201

Lack of a Zn/Co substitution ability in the polar diatom *Chaetoceros neogracile* RS19

Riss M. Kellogg ¹⁰, ¹ Dawn M. Moran, ² Matthew R. McIlvin, ² Adam V. Subhas ¹⁰, ² Andrew E. Allen, ³ Mak A. Saito ¹⁰ ^{2*}

¹MIT/WHOI Joint Program in Oceanography/Applied Ocean Science and Engineering, Cambridge, Massachusetts

Abstract

Functional substitution of the essential trace metals zinc (Zn) and cobalt (Co) within metalloenzymes has been well documented in marine diatoms and is known to be prevalent among varying genera and species. In contrast to the majority of species studied to date, we find that the polar diatom *Chaetoceros neogracile* RS19, originally isolated from the Ross Sea, Antarctica, has a Zn requirement that cannot be met by Co and thus does not demonstrate a Zn/Co substitution ability as assessed by growth rate. We investigated this diatom's inability to use Co to alleviate Zn-limited growth rates at the transporter, sensor/chaperone, and metalloenzyme level using metal quota and proteomic analyses of cultures grown over a range of Zn and Co availability. Analysis of total cellular metal quotas revealed that, although incapable of substitution, this diatom still actively assimilated dissolved Co. We furthermore observed distinct trends in the abundance levels of putative α and θ -CAs, ZIP transporters, Zn fingers, and a Zn chaperone in response to increasing media Zn²⁺. Overall, Co appears to be transported into the cell, but not efficiently utilized by Zn metalloenzymes.

Zinc (Zn) is an important trace element in algal metabolism due to its use as a cofactor in Zn-containing metalloenzymes such as carbonic anhydrases (CAs), which are key parts of the carbon concentrating mechanism (CCM) in aquatic photoautotrophs (Badger and Price 1994; Badger et al. 1998; Espie and Colman 2005; Jensen et al. 2020). Intracellular CAs catalyze the interconversion of accumulated HCO_3^- to CO_2 in proximity to Rubisco and prevent CO_2 leakage from the cell (Badger 2003) while extracellular CAs associated with the plasma membrane, periplasmic space, or cell wall are thought to facilitate CO_2 influx by converting HCO_3^- to CO_2 within the diffusive boundary layer surrounding the cell (Moroney et al. 1985; Elzenga et al. 2000; Burkhardt et al. 2001; Hopkinson et al. 2013).

*Correspondence: msaito@whoi.edu

Additional Supporting Information may be found in the online version of this article.

Author Contribution Statement: All authors contributed to data acquisition and analysis. R.M.K. designed and implemented the study. D.M.M. originally isolated *Chaetoceros* RS19 used in this study and maintained cultures. M.R.M. assisted with proteomic analyses. A.E.A. contributed the translated metatranscriptome for *Chaetoceros* RS19 used as a reference database for proteomic analyses. R.M.K., A.V.S. and M.A.S. wrote the manuscript. All authors approved the final submitted manuscript.

To date, seven subclasses of CA (α, β, γ, δ, ζ, θ, and ι) have been identified in marine phytoplankton (DiMario et al. 2018; Jensen et al. 2019), none of which share homology and are thus thought to be the result of convergent evolution (Hewett-Emmett and Tashian 1996; So et al. 2004). While Zn^{2+} is the cofactor most commonly used in algal CAs, utilization of both cadmium (Cd²⁺) and cobalt (Co²⁺) in place of Zn^{2+} has been previously documented in the diatom *Thalassiosira weissflogii* via the use of ζ-CA (CDCA) and δ-CA (TWCA1) that are able to replace Zn^{2+} with Cd²⁺ and with Co²⁺, respectively (Price and Morel 1990; Lee and Morel 1995; Yee and Morel 1996; Lane and Morel 2000a; Lane et al. 2005).

It is well established that the addition of Co²⁺ (or Cd²⁺) can restore the growth rate of many Zn²⁺-limited marine algal species in culture, and the major mechanism for this restoration is thought to be due to the replacement of Zn²⁺ by Co²⁺ or Cd²⁺ in CAs (Morel et al. 2020). This substitution effect has been investigated by measuring specific culture growth rates with variations in Zn and Co concentrations added to the growth media (Sunda et al. 2005; Haas et al. 2009; Kellogg et al. 2020) and has been documented in a variety of marine diatom species including *Thalassiosira pseudonana, Thalassiosira oceanica, T. weissflogii, Thalassiosira* sp. UNC1203, *Phaeodactylum tricornutum,* and *Pseudo-nitzschia delicatissima* UNC1205 (Sunda and Huntsman 1995; Haas et al. 2009; Kellogg et al. 2020) as well as in the marine prymnesiophytes *Emiliania huxleyi* and

²Department of Marine Chemistry and Geochemistry, Woods Hole Oceanographic Institution, Woods Hole, Massachusetts

³Scripps Institution of Oceanography, Integrative Oceanography Division, University of California, San Diego, La Jolla, California

Phaeocystis antarctica (Sunda and Huntsman 1995; Timmermans et al. 2001; Xu et al. 2007; Saito and Goepfert 2008).

Although many marine diatom species are capable of metabolic Zn/Co inter-replacement to some degree, notable exceptions within the genus Chaetoceros exist. Both Chaetoceros calcitrans and Chaetoceros simplex are reportedly unable to alleviate Zn-limited growth rates using Co (Timmermans et al. 2001; Koch and Trimborn 2019). Zn/Co metabolic substitution therefore does not appear to be universal among diatoms, and based on these studies, members of the genus Chaetoceros appear incapable of substituting Co in place of Zn. To further explore this inability within the genus Chaetoceros, we conducted Zn and Co addition experiments on a Southern Ocean (Ross Sea) isolate of the polar diatom Chaetoceros neogracile RS19 and analyzed the growth rate, metal quota and proteomic response to metal addition. Like C. calcitrans and C. simplex, we find that C. neogracile RS19 also possesses an absolute Zn requirement for growth that cannot be replaced by Co. This study examines the influence of Zn and Co nutrition on the specific growth rate, total metal content, and proteome of a substitution-incapable diatom in order to explore possible mechanisms underlying the inability to Zn/Co substitute.

Materials and methods

Media and culturing techniques

C. neogracile RS19 cultures were maintained in a 4°C incubator under constant cool white fluorescent lighting (30 µmol photon m⁻² s⁻¹). All cultures were randomly repositioned each day to avoid any effect of subtle variation in light intensity on growth. C. neogracile RS19 was originally collected from the Ross Sea, Antarctica, and was isolated on 26 June 2000 by D. Moran. Species-level identification was performed with 18S rRNA gene sequence analysis (GenBank accession EF432514.1) and had 99.9% sequence overlap (1697/1699 base pairs) with the 18S sequence from C. neogracile (NCBI accession EU090012.1). Stock cultures of this isolate were maintained continuously in the Saito laboratory at the Woods Hole Oceanographic Institution. All cultures were axenic and maintained by sterile technique until needed. Microscopy images were obtained using a Zeiss Axio Imager A2 microscope using differential interference contrast optics (Fig. S5).

All polycarbonate culture tubes and other plasticware used in the experiments were cleaned to remove trace metal contaminants before use. This procedure involved, at minimum, a 72 h soak in < 1% Citranox detergent, five rinses in Milli-Q water, a 7 d soak in 10% HCl, and five rinses with dilute acid (HCl, pH 2). Biological duplicate cultures were grown over 12 metal treatments in microwave-sterilized 28 mL polycarbonate centrifuge tubes (Nalgene) containing 25 mL total media. All solutions were pipetted after a tip rinse procedure consisting of three rinses with 10% HCl followed by three rinses with sterile dilute HCl (pH 2). All culture work was

conducted in a Class 100 clean room and transferring of cultures was conducted in a laminar flow hood within the clean room.

Culture media was prepared after that used by Sunda and Huntsman (1995, 2005) for trace metal experimentation. Microwave sterilized (Keller et al. 1988) 0.2 μm-filtered Equatorial Pacific surface seawater collected at station 14 of the 2016 ProteOMZ expedition (10.5600°S, 146.3133°W; cruise code FK160115) was used as the media base. Macronutrients were added to this sterile base to a final concentration of 88.2 μ M NaNO₃, 41.5 µM NaH₂PO₄, and 106 µM Na₂SiO₃. Macronutrient stock solutions were Chelex-treated to remove trace metal contaminants before use (Sunda et al. 2005). Added vitamins included 2 nM biotin, 0.37 nM B₁₂ as cyanocobalamin, and 300 nM thiamine and were also Chelex-treated before use. Trace elements were added to final media concentrations of 10^{-7} M FeCl_3 , $4.8 \times 10^{-8} \text{ M MnCl}_2$, $4.0 \times 10^{-8} \text{ M CuSO}_4$, 10^{-7} M NiCl₂, and 10^{-8} M Na₂O₃Se within a 10^{-4} M ethylenediamine tetraacetic acid disodium salt (EDTA, Acros Organics, C₁₀H₁₄N₂Na₂O₈) metal ion buffer system (Sunda et al. 2005). All media amendments were sterile filtered through acid-rinsed 0.2-µm filters before addition to final media. Media were equilibrated for at least 12 h before inoculation.

Established cultures were first acclimated in low-metal media containing 1 nM total added Zn or less for at least three transfers. These acclimated cultures were used as a 1% inoculum for biological duplicate experimental cultures. All growth media was chilled to the experimental temperature (4°C) before inoculation. For Zn limitation experiments, media was amended with 0, 1, 3, 10, 30, and 100 nM total added Zn in the absence of added Co. Similarly for Co limitation experiments. Co was added at the same concentrations in the absence of added Zn. We refer to growth rate experiments using media amended with Zn or Co (while omitting the other) as "simple limitation" experiments. Growth rate experiments in which one metal was held at a constant total added value while varying the added concentration of the other metal were also conducted—we refer to these as "double addition" experiments. Growth of all experiment cultures was monitored by relative chlorophyll fluorescence using a Turner TD-700 fluorometer, calibrated prior to measurement with a solid standard. All cultures were grown in 28 mL polycarbonate tubes (see above) that are compatible with the fluorometer. This allowed measurements to be taken for the entire culture without having to take subsamples, mitigating the risk of exposing cultures to contamination. Growth rates were calculated from the slope of the natural log of chlorophyll fluorescence vs. time during exponential growth over a 6-d period. Computed ratios of $[Zn^{2+}]$ and $[Co^{2+}]$ to total concentrations, whose values are $10^{-3.99}$ and $10^{-3.63}$, respectively, were used to convert total added metal concentrations to free ion concentrations and are the same as those used by Sunda and Huntsman (1995).

There is a body of literature involving physiological, multielement trace metal studies relying on singlicate measurements (Sunda and Huntsman 1995, 1998a, 2000, 2005). The use of replication in multi-element studies is difficult because the number of treatments can become unwieldy for experimentation in a single incubator chamber, for example a 6×6 matrix of treatments is 36, 72, or 108 experimental flasks, in singlicate, duplicate, or triplicate, and hence increased replication often comes at the expense of exploration of multiparameter space. It is thought that trace metal physiology is less prone to biological variability due to the use of cleanrooms and lack of dust contamination that is ubiquitous in non-cleanroom experiments. In this study, we chose to use biological duplicates. The relative standard deviation of the range of variability in growth rate for all values in Table S1 was 1.8%, consistent with the notion that cleanroom-based trace metal physiology is highly reproducible.

Metal quotas

Cellular metal quotas were measured by inductively coupled plasma mass spectrometry (ICP-MS). Biomass from biological duplicate 25 mL double addition cultures of C. neogracile RS19 were pooled upon reaching late log phase of growth and were centrifuged at 11,000 RPM (14,610g) for 40 min at 4°C. The cell pellet was resuspended in ~ 1 mL media and transferred to an acid-cleaned microcentrifuge tube. Cultures were centrifuged again for 30 min at 14,100 RPM (13,336g) at 4°C before the supernatant was discarded. Half of the remaining cell pellet was acidified in 800 μ L of 5% nitric acid (Optima) containing 1 ppb indium for at least 7 d while the other half was retained for proteomic analysis. Solids were removed by centrifugation. No attempt was made to remove extracellular metals by washing cells with additional metal chelators in order to minimize processing blanks. Quota determinations therefore include contributions from both intracellular and extracellular pools. Process blanks containing acid but no cells were digested as samples were. Digests were diluted by a factor of 9 with 5% nitric acid 1 ppb indium solution before being analyzed in technical duplicate on a Thermo ICAP-Q plasma mass spectrometer calibrated to a multi-element standard curve (Spex Certiprep) over a range of 1–20 ppb ($R^2 \ge 0.9998$ for all metal standard curves). Samples were analyzed in KED mode after an 85 s sample uptake window and element mass windows were scanned three times during measurements. The 1 ppb indium internal standard was used to correct for variation in sample delivery and plasma suppression between samples. Process blanks were subtracted from measured concentrations. Phosphorus concentrations were also measured by ICP-MS simultaneously and were calibrated to a standard curve ranging from 100-3200 ppb $(R^2 = 0.9999)$ using a 1 ppm certified P stock (Alfa Aesar Specpure). The seawater media base used for all growth experiments was similarly analyzed via ICP-MS using a 1:10 dilution of media base into 5% nitric acid 1 ppb indium and analyzed as above to determine background media concentrations of total Zn and Co (0.7 and 0.1 nmol L⁻¹, respectively). The steady-state net uptake rates (ρ) of Fe, Mn, Ni, Cu, Zn, Cd, and Co were also calculated as the cellular metal quota (Q) multiplied by the specific growth rate (μ) of double addition cultures (Sunda and Huntsman 1995). The metal quota sample corresponding to the Zn²⁺ = 1e–13 M treatment was contaminated and therefore not included.

Proteomic analysis of experiment cultures

Biomass from biological duplicate 25 mL cultures was collected during late log phase growth for proteomic analysis by centrifugation at 11,000 RPM (14,610g) for 40 min at 4°C. Proteins were extracted, alkylated and reduced using a modification of previously published methods (Saito et al. 2011; Hughes et al. 2014). Biomass was resuspended in lysis buffer (50 mM HEPES, pH 8.5, 1% SDS) and heated for 10 min at 95°C, then incubated for 30 min at room temperature with gentle shaking at 350 RPM. Biomass was then centrifuged at 14,100g for 20 min to remove cellular debris. The supernatant was transferred to an ethanol-washed microcentrifuge tube and 2 µL of benzonase nuclease was added before incubating for 30 min at 37°C. Samples were then alkylated by adding $5 \mu L$ of 200 mM dithiothreitol (DTT) in 50 mM HEPES pH 8.5 per 100 µL of lysate and incubated at 45°C for 30 min. Ten microliters of 400 mM iodoacetamide in 50 mM HEPES pH 8.5 was then added, followed by incubation in the dark for 30 min at 24°C. Ten microliters of 200 mM DTT in 50 mM HEPES pH 8.5 per $100 \mu L$ of lysate was then added to quench the reaction.

Proteins were isolated and washed using a magnetic bead method adapted from Hughes et al. (2014), using a 1:1 mixture of hydrophobic and hydrophilic Sera-Mag SpeedBeads (GE Healthcare Life Sciences). Magnetic beads were added to the protein mixture at a concentration of 20 μ g/100 μ L of total reaction. The solution was acidified with 10% formic acid to pH 2. Acetonitrile (ACN) was then immediately added to a final concentration of 50% and samples were incubated for 15 min at 37°C, then for 30 min at room temperature before being placed on magnetic racks for 2 min. The mixture was then washed with an equal volume of 70% ethanol (2 \times) and ACN $(1\times)$. After removing the final ACN wash, the proteins were reconstituted in 50 mM HEPES (pH 8.0) and trypsin digested for 14 h at 37°C. The mixture was resuspended, washed with ACN, and placed on the magnetic rack. Proteins adhered to beads while ACN was removed by pipetting. The peptide sample was reconstituted in 2% DMSO and acidified with 1% formic acid to bring to a final concentration of 0.1 µg/µL. Protein concentration was quantified using a colorimetric assay at 562 nm (BCA total protein assay; Thermo Fisher Scientific).

Whole cell protein digests were analyzed in technical duplicate by liquid chromatography mass spectrometry (LC–MS) using a Paradigm MS4 HPLC system (Michrom) with reverse

phase chromatography, a Michrom ADVANCE source, and a Thermo Scientific Q Exactive hybrid quadrupole-orbitrap mass spectrometer. Mass spectra were searched against a C. neogracile RS19 translated transcriptome database (see Data Availability section) that was generated under iron limitation and otherwise replete conditions using Proteome Discoverer's SEQUEST algorithm (Thermo Fisher Scientific) with a fragment tolerance of 0.02 Da and parent tolerance of 10 ppm. Database search results were processed and visualized using spectral counting abundance scoring within Scaffold 4.0 (Proteome Software, Inc.). Protein abundances are reported as total normalized spectra with the following parameters: 99.0% minimum peptide threshold, 99.0% minimum, and three peptides minimum protein threshold, 0.0% peptide false discovery rate (FDR), and 0.0% protein FDR. A total of 285,535 mass spectra were detected from 12 biological samples, resulting in 1064 protein identifications. Of these proteins, 814 had PFam annotations.

Protein BLAST searches

The stand-alone command line application BLAST+ from the National Center for Biotechnology Information was used to identify CAs in the proteome of C. neogracile RS19 generated in this study. The proteome was BLAST searched (E = 5e-5) against a custom database of known diatom CAs that included eight α , two β , seven γ , five δ (including TWCA), two ζ (including CDCA), one θ , and one 1-CA from the marine diatoms T. pseudonana, P. tricornutum, and T. weissflogii (Table S4). Alignments are shown in Fig. S1. Representative protein members of the metal transporter families Zrt/Irt-like (ZIP), cation diffusion facilitators (CDFs), P1B-type ATPases, and vacuolar iron transporter 1 (VIT1) were similarly searched for within the proteome using BLAST+. Sequences of representative metal transport proteins from T. pseudonana and P. tricornutum were acquired from annotated proteomic databases (Thaps3 and CCAP 1055/1 v2.0 Phatr2, all models) available online from the Joint Genome Institute (jgi.doe.gov) (Armbrust et al. 2004; Bowler et al. 2008) (Table S6). Transmembrane domains in *C. neogracile* proteins were predicted with TMHMM Server v.2.0 (http://www.cbs.dtu.dk/services/TMHMM-2.0/) (Krogh et al. 2001).

Statistics and visualizations

Half-saturation constants $(K_{\rm m})$ for growth and maximal growth rates (μ_{Max}) were calculated from simple limitation growth rates using a nonlinear fitting function in MATLAB v. R2020b (MathWorks Inc.). Relationships between protein spectral counts, specific growth rates, and Zn metal quotas were analyzed using two-way least squares linear regressions performed in MATLAB using the script lsqfitma.m (Glover et al. 2011). A paired t-test comparing growth rates achieved in simple Zn limitation and in Zn double addition experiments was performed in MATLAB at a 1% significance level ($\alpha = 0.01$). Protein alignments were generated in MEGAX 10.1 using the MUSCLE multiple sequence alignment program with default parameters (Edgar 2004; Kumar et al. 2018). Statistical analysis of selected proteomes represented by volcano plots was conducted using a paired two-way t-test in MATLAB with a significance cutoff of p < 0.05. Average spectral count values of zero were changed to a small value (0.1) to allow for fold change estimates. Proteomic heatmaps were generated in R v.4.0.3 using pheatmap v1.0.12, with spectral counts normalized using the normalized spectral abundance factor (NSAF) calculation (Zhang et al. 2010). NSAF-normalized spectral counts assigned to redundant PFam annotations were summed together.

Results

Growth rate experiments

In simple Zn^{2+} limitation, increasing Zn^{2+} concentrations resulted in increased growth rates in *C. neogracile* RS19 to a maximum of $0.43 \, d^{-1}$ (Fig. 1a, blue data points; Table S1).

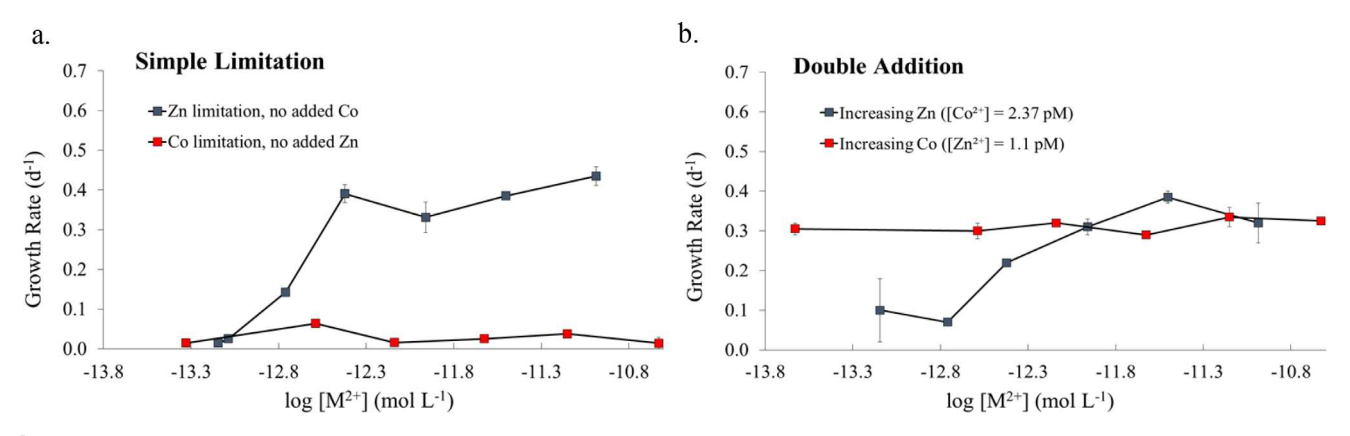


Fig. 1. (a) Growth rates of *Chaetoceros neogracile* RS19 for simple limitation experiments varying zinc concentrations with no added cobalt (Zn limitation, no added Co) and varying cobalt concentrations with no added zinc (Co limitation, no added Zn). (b) Growth rates for double addition experiments in which the concentration of one element varies while the other is held constant. Growth rate values are means \pm range for biological duplicate cultures. Data plotted from Table S1.

A $K_{\rm m}$ of 2.9×10^{-13} M for Zn²⁺ was calculated from simple limitation growth rates using nonlinear Monod curve fitting ($R^2=0.87$), and is in good agreement with the $K_{\rm m}$ (Zn²⁺) value reported for *C. calcitrans* (1.9×10^{-13} M; Timmermans et al. 2001) and for the diatoms *P. delicatissima* UNC1203 (1.96×10^{-13} M) and *T. pseudonana* CCMP1335 (5.11×10^{-13} M) (Kellogg et al. 2020). In simple Co²⁺ limitation, growth rates remained < 0.1 d⁻¹ irrespective of how much Co was added (Fig. 1a, red data points; Table S1) indicative of an inability to use Co to alleviate Zn-limited growth.

Lack of a substitution ability in *C. neogracile* RS19 was further demonstrated in the double addition experiments, in which one metal was held at a constant value while the concentration of the other metal increased. With increasing Zn²⁺, and Co²⁺ held constant at 2.37 pM, growth rates increased to a maximum of 0.39 d⁻¹ (Fig. 1b, blue data points; Table S1). This growth rate is similar to the maximum of 0.43 d⁻¹ achieved with simple Zn addition (Fig. 1a, blue data points). In the converse scenario, with a Zn²⁺ concentration held constant at 1.1 pM, increasing Co²⁺ resulted in highly uniform growth rates (~ 0.32 d⁻¹) over the entire range of added Co

(Fig. 1b, red data points). Growth rates achieved with 1.1 pM $\rm Zn^{2+}$ and various amounts of additional Co ($\sim 0.32~\rm d^{-1}$) were therefore nearly identical to the growth rate achieved with 1.1 pM $\rm Zn^{2+}$ with no additional Co (0.33 d⁻¹) (Fig. 1b; Table S1). Increasing $\rm Zn^{2+}$ concentrations thus determined the growth response of *C. neogracile* RS19, with Co²⁺ having no effect or slightly negative effects on growth rate.

Cellular metal quotas

Upon reaching late log phase of growth, biomass from biological duplicate double addition cultures of *C. neogracile* RS19 was pooled, harvested, and analyzed for total cellular Fe, Mn, Ni, Cu, Zn, Cd, and Co metal content. Metal quotas normalized to cellular phosphorus (P) content are listed in Table S2 and shown in Fig. 2a. Distinct differences in quota trends were apparent when comparing Co^{2+} amended cultures with Zn^{2+} amended cultures. We observed comparatively smaller variations in Fe : P, Mn : P, Ni : P, Cu : P, Zn : P, and Cd : P quotas across all Co amendments (Fig. 2), with averages of 6.01 ± 0.39 mmol Fe mol $^{-1}$ P, 6.55 ± 0.53 mmol Mn mol $^{-1}$ P, 0.06 ± 0.012 mmol Ni mol $^{-1}$ P, 0.06 ± 0.003 mmol Cu mol $^{-1}$ P, 0.06 ± 0.003 P, 0.06 ± 0.003

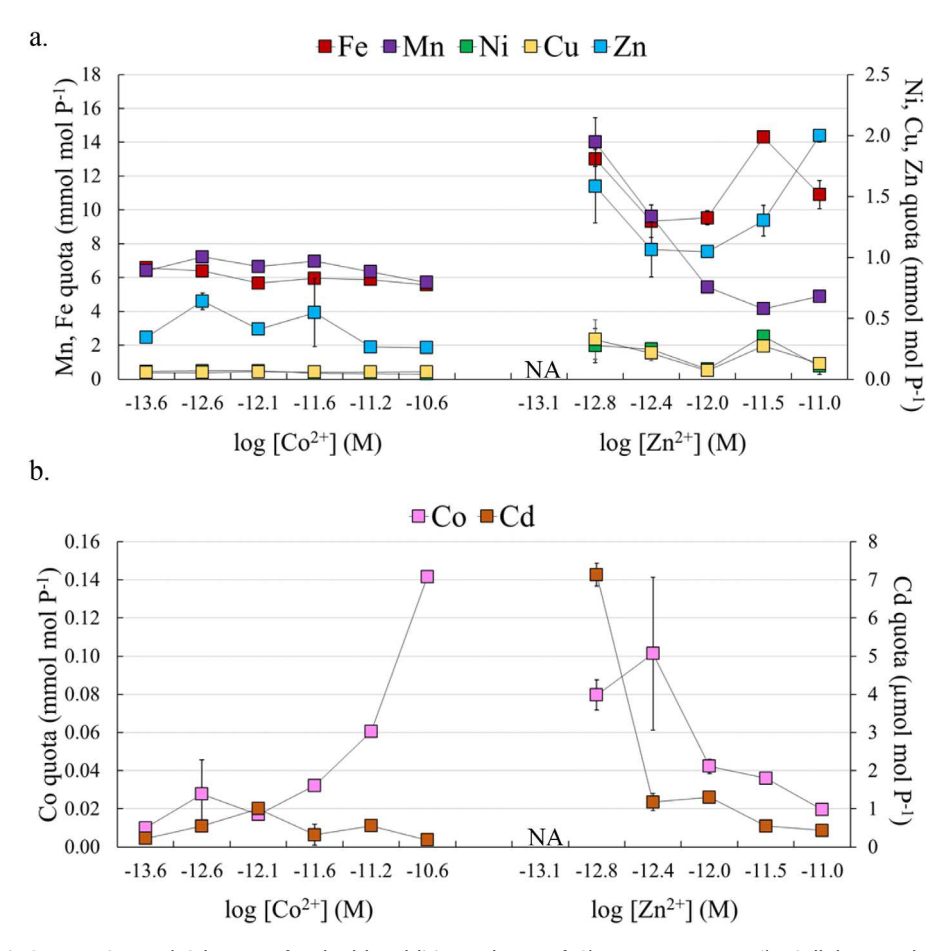


Fig. 2. Cellular Fe, Mn, Ni, Cu, Zn, Co, and Cd quotas for double addition cultures of *Chaetoceros neogracile*. Cellular metal quotas are normalized to cellular P. Data plotted from Table S2. Quota values were analyzed from pooled biological duplicate cultures. Mean values are plotted \pm the range of technical duplicate measurements for each treatment. NA, not available.

 0.41 ± 0.15 mmol Zn mol⁻¹ P, and $0.47 \pm 0.30~\mu$ mol Cd mol⁻¹ P, respectively (Fig. 2a,b; Table S2). Only Co quotas demonstrated a distinct trend, with increased quotas under increasing added Co²⁺. A minimum Co quota of 0.01 mmol mol⁻¹ P at [Co²⁺] = 0.02 pM and a maximum quota of 0.14 mmol mol⁻¹ P at [Co²⁺] = 23.47 pM was observed (Fig. 2b; Table S2).

In the converse scenario of metal additions, with Co²⁺ held constant at 2.37 pM while Zn²⁺ increased, no trends were apparent in Fe, Ni, and Cu quotas, though maximum quota

values were generally higher than those achieved in added Co (Fe $_{Q,Max}=14.3$ mmol mol P^{-1} at $[Zn^{2+}]=3.14$ pM, $Ni_{Q,Max}=0.35$ mmol mol P^{-1} at $[Zn^{2+}]=3.14$ pM, $Cu_{Q,Max}=0.33$ mmol mol P^{-1} at $[Zn^{2+}]=0.17$ pM) (Fig. 2; Table S2). An overall decrease in Mn quotas was observed, with a maximum of 14.01 mmol mol P^{-1} at $[Zn^{2+}]=0.17$ pM and a minimum of 4.16 mmol mol P^{-1} at $[Zn^{2+}]=3.14$ pM. As added Zn increased, Zn quotas increased to a maximum of 2.0 mmol mol P^{-1} at $[Zn^{2+}]=10.3$ pM. Decreases in Co : P and Cd : P quotas were

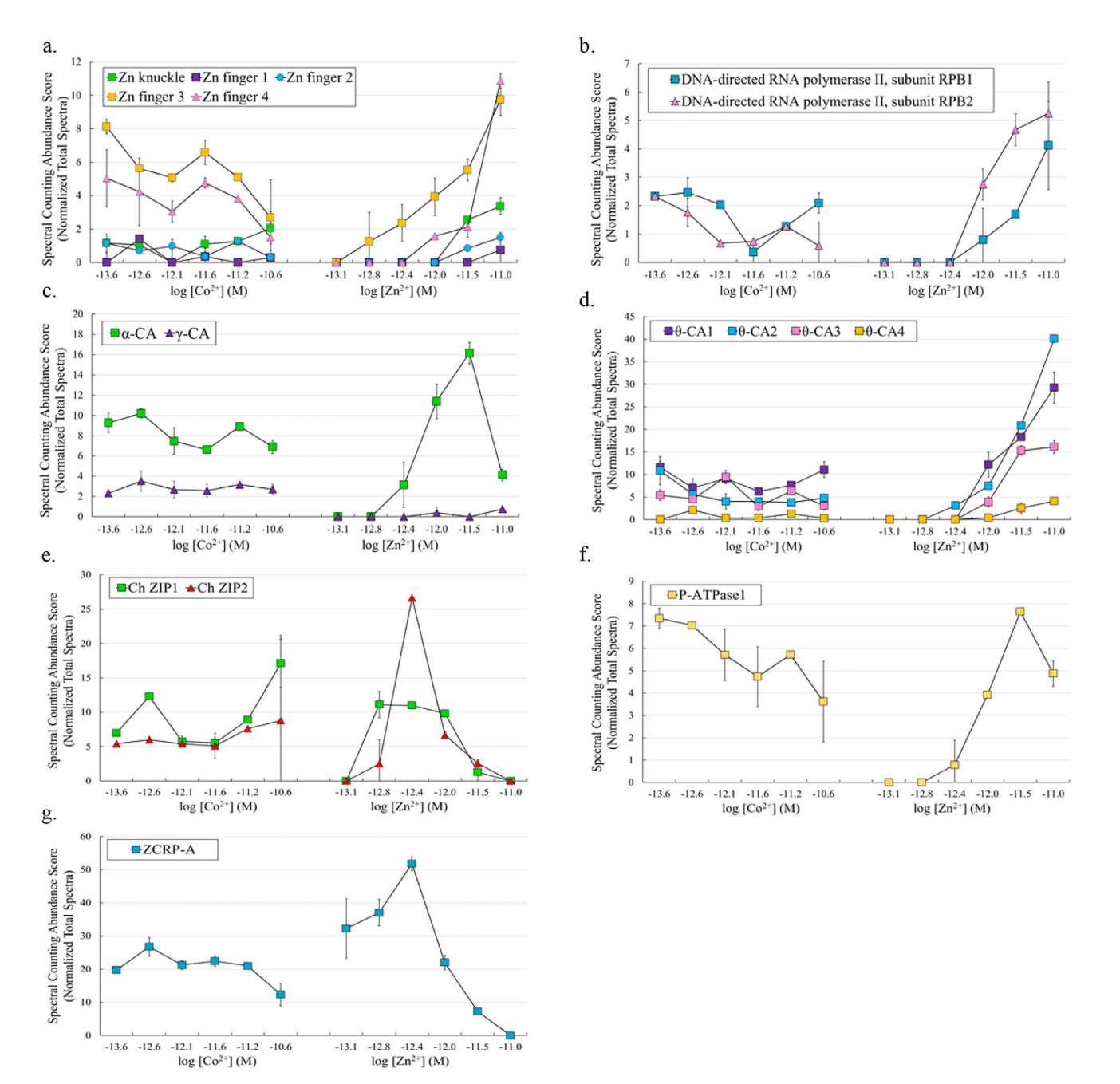


Fig. 3. Mean spectral counting abundance scores of putative (a) Zn fingers, (b) RNA polymerases, (c) alpha, gamma, and (d) theta carbonic anhydrases (CAs), (e) ZIP transporters, (f) P-ATPase, and (g) ZCRP-A detected in double addition proteomes of *Chaetoceros neogracile* RS19. Mean abundance scores were analyzed from pooled biological duplicate cultures. Mean values are plotted \pm the range of technical duplicate measurements for each treatment.

also observed with increasing Zn, with minimum quotas of both metals (0.019 mmol Co mol P^{-1} and 0.43 μ mol Cd mol P^{-1}) observed at the largest added Zn treatment, $[Zn^{2+}] = 10.3$ pM.

Detection and analysis of Zn regulatory and RNA polymerase proteins

Proteomic analysis of *C. neogracile* RS19 biomass was conducted to explore the abundance patterns of Zn-related proteins expressed in this diatom in response to Zn and Co nutrition. Beyond its role as a catalytic cofactor in metalloproteins, Zn also performs roles in DNA-directed RNA polymerases and in cellular regulatory processes via zinc fingers, small Zn-binding domains within various proteins functioning in transcription and translation (Krishna 2003). Increases in five distinct Zn finger proteins (including one Zn knuckle) were observed with increasing Zn^{2+} (Fig. 3a). Two subunits of RNA polymerase II were also identified within the proteomic data, with increasing abundances of both subunits with increasing Zn^{2+} , but not with increasing Co^{2+} (Fig. 3b).

Detection and analysis of CAs

As diatoms are known to possess CAs that retain functionality with both Zn^{2+} and with Co^{2+} , we next investigated the CA portfolio of *C. neogracile* RS19. Using the application BLAST+, CAs were identified by searching the generated *C. neogracile* RS19 proteomes against a custom database of

known diatom CAs that included eight α , two β , seven γ , five δ (including TWCA), two ζ (including CDCA), one θ , and one 1-CA from the marine diatoms T. pseudonana, P. tricomutum, and T. weissflogii (Table S5). Six C. neogracile RS19 proteins were identified as putative CAs based on sequence homology, including one α -CA, one γ -CA, and four θ -CAs (Figs. 3c,d, S1; Table S5). Distinct expression patterns of the α -CA and of θ -CA1, θ -CA2, and θ -CA3 in units of total spectral counts as a function of increasing Zn^{2+} or increasing Zn^{2+} were observed. With increasing Zn^{2+} , the abundances of these CAs showed little variation. In contrast, with increasing Zn^{2+} , the abundance of these CAs markedly increased (Fig. 3c,d). Abundances of only two out of the six detected CAs, γ -CA and θ -CA4, were not significantly different across all Zn treatments (paired two-way t-test, p = 0.05).

Detection and analysis of putative metal transporters

In addition to CAs, representative protein members of the metal transporter families Zrt/Irt-like (ZIP) and P1B-type ATPases were also identified by searching the *C. neogracile* RS19 proteome using BLAST+. Two proteins henceforth referred to as Ch ZIP1 and Ch ZIP were identified as ZIP transporters based on sequence similarity to a known ZIP transporter in *T. pseudonana* (Figs. 3e, S2a; Table S6). With Zn²⁺ held constant at 1.1 pM while Co²⁺ increased, maximum spectral counts of both Ch ZIP1 and Ch ZIP2 were observed at

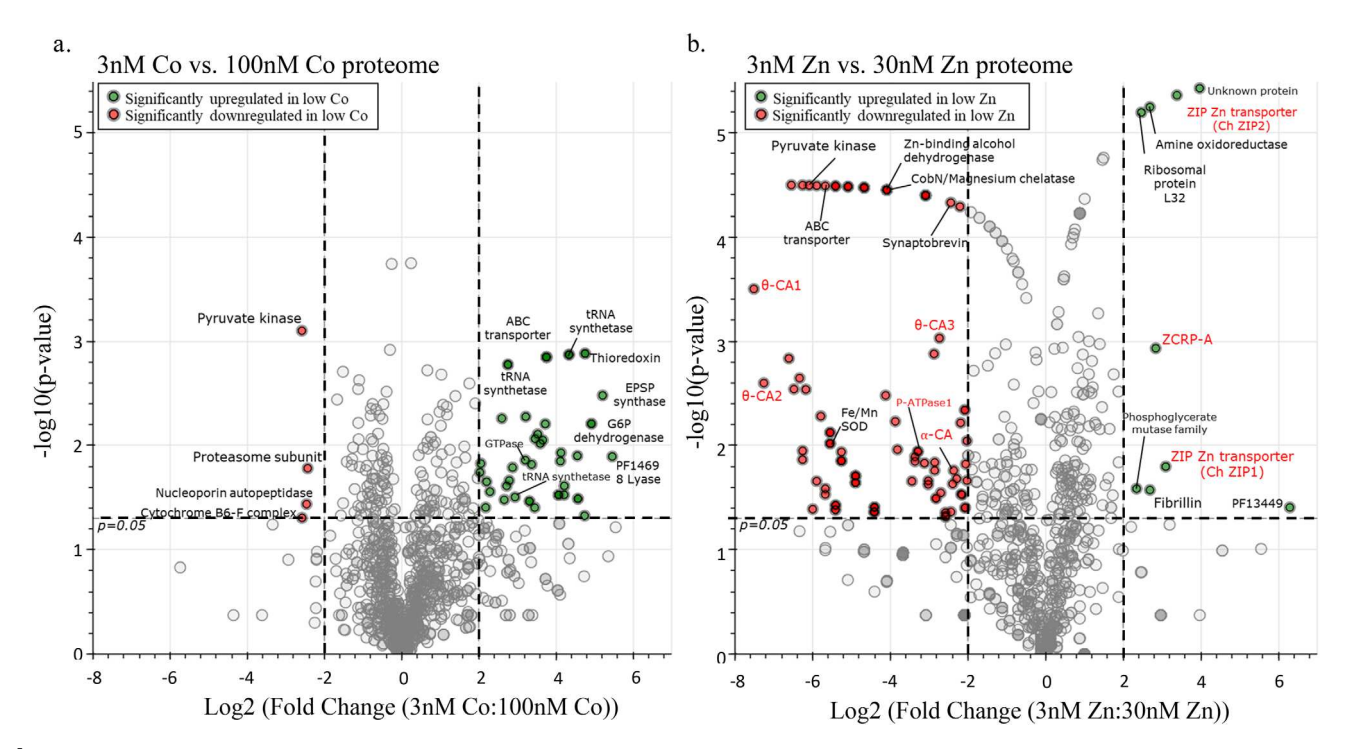


Fig. 4. Volcano plots showing the distribution of quantified *Chaetoceros neogracile* proteins according to p value and fold change comparing (a) a low vs. high added Co treatment and (b) a low vs. high added Zn treatment. Dashed lines indicate significance level cutoffs at p < 0.05 and $|\log 2|$ fold change | > 2. Protein names in red text are those proteins of interest described in Tables S5 and S6 and plotted in Fig 3. Values of zero were changed to a small value (0.1) to allow for fold changes estimates.

19395590, 2022

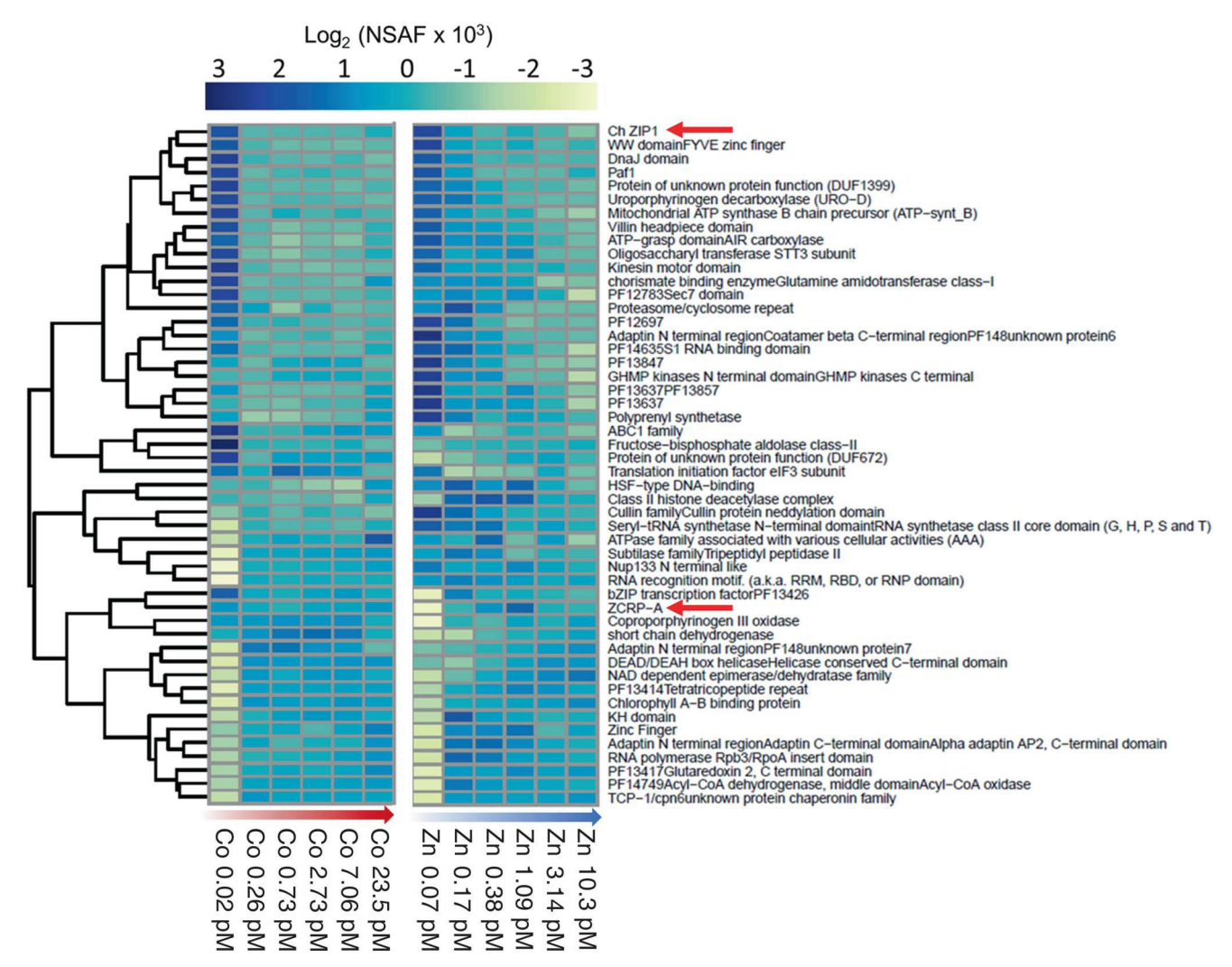


Fig. 5. Heatmap of log₂ NSAF-normalized *Chaetoceros neogracile* protein spectral counts showing relative protein abundance at the PFam annotation level. The top 50 PFam-annotated genes with highest deviations from the mean (variances) across all double addition cultures are shown. The dendrogram shows similarity in spectral abundance among samples based on Euclidean distance and hierarchical clustering. Each row represents a PFam annotation, with spectral counts associated with identical PFams summed together. Color gradients represent low (yellow) to high (blue) protein expression.

the highest Co^{2+} concentration (17 and 9 counts, respectively; $[\text{Co}^{2+}] = 23.47 \text{ pM}$; Fig. 3e). In contrast, with Co^{2+} held constant at 2.37 pM while Zn^{2+} increased, both ZIP transporters demonstrated similar behavior. Both were undetectable at the lowest and highest Zn^{2+} concentrations (0.07 and 10.3 pM, respectively) and exhibited maximum values at intermediate Zn^{2+} concentrations, centering on $\text{Zn}^{2+} = 0.4 \text{ pM}$ (Fig. 3e).

A protein henceforth referred to as P-ATPase1 was identified as a putative P-ATPase based on BLAST similarity to the cellular Cd^{2+} efflux protein ATPase5-1B in *P. tricornutum* (Fig. S2b; Table S6). P-ATPase1 spectral counts showed an overall decreasing trend with increasing Co^{2+} (Fig. 3f). In contrast, spectral counts ranged from undetected at the two lowest Zn^{2+} treatments to a maximum of 8 at $[Zn^{2+}] = 3.1$ pM (Fig. 3f). In addition, we note the increased expression of the

putative metal chaperone ZCRP-A under low Zn as observed previously in *C. neogracile* RS19 and in other marine diatoms (Kellogg et al. 2022). Similar to CA abundance trends, total ZCRP-A spectral counts were not modulated by increasing $[\text{Co}^{2+}]$ (Fig. 3g).

To investigate the response of *C. neogracile* RS19 to low vs. high added metal concentrations at the whole-proteome level, we compared proteomes generated under 3 vs. 100 nM total added Co and under 3 vs. 30 nM total added Zn using volcano plots (Fig. 4). Notably, the abundance levels of all CAs and transporters investigated in this study (Tables S5, S6) were not significantly different comparing low vs. high Co additions (Fig. 4a). In contrast, comparison of proteomes generated under low vs. high added Zn revealed the significant upregulation of both ZIP transporters, Ch ZIP1 and Ch ZIP2,

19395590, 2022

Kellogg et al.

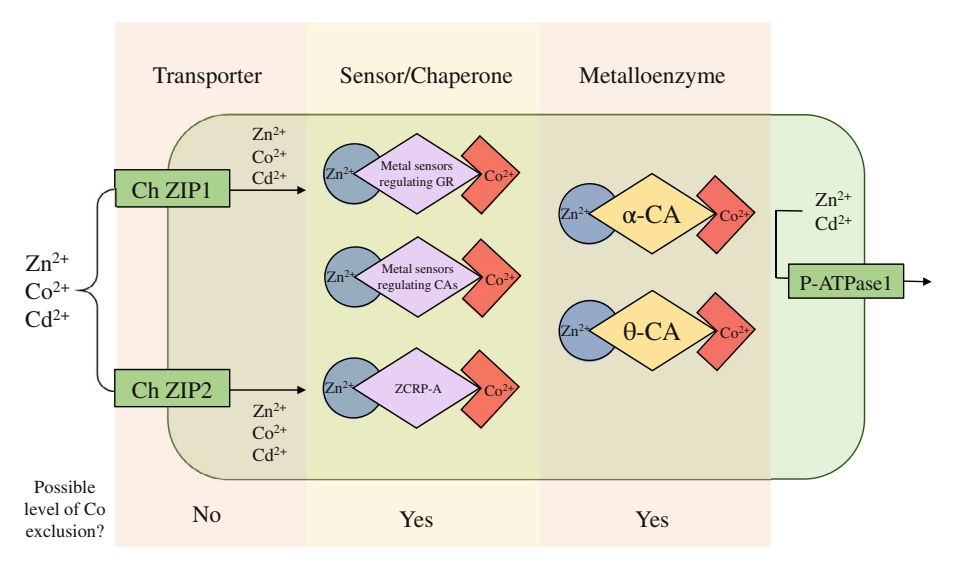


Fig. 6. Cartoon schematic illustrating possible mechanisms of Co exclusion at the transporter, sensor/chaperone, and metalloenzyme level in *Chaetoceros neogracile*, highlighting the proteins investigated in this study. ZIP, Zrt/Irt-like metal transporter; GR, growth rate; CA, carbonic anhydrase; ZCRP-A, zinc-cobalt responsive protein A.

as well as the putative metal chaperone ZCRP-A (Fig. 4b, green data points) and the significant downregulation of α -CA, three θ -CAs, and P-ATPase1 under low Zn (Fig. 4b, red data points). A heatmap comparing the top 50 proteins with highest variances in spectral abundance scores across all samples also revealed the increased abundance of ZCRP-A under low Zn and the upregulation of the Ch ZIP1 transporter under low added metal conditions (Fig. 5).

Discussion

While the ability to use Co to restore Zn-limited growth rates appears to be a widely shared capability among marine phytoplankton, a few exceptions have been found. Two species of Chaetoceros, C. calcitrans (CCMP1315; location of isolation unknown) and C. simplex (CS 624, ANACC; isolated from Prydz Bay, Antarctica), appear to be incapable of substituting Co in place of Zn (Timmermans et al. 2001; Koch and Trimborn 2019). Our results confirm this to be true for another polar, psychrophilic Chaetoceros species, C. neogracile RS19. We further explored the underlying mechanisms that create this behavior using metal quota and proteomic analyses. Together these results provide a better understanding of the metal homeostasis and selectivity within this representative member of the ecologically relevant Southern Ocean genus Chaetoceros (Leventer 1991; Kang et al. 2001; Lasbleiz et al. 2016).

We have demonstrated that C. neogracile RS19 is incapable of using Co to restore Zn-limited growth rates, as growth rates were not stimulated by increasing Co^{2+} concentrations up to 23.5 pM in the absence of added Zn (Fig. 1a). This behavior is different from that observed in many other diatoms (and other algal genera) for which Co addition clearly stimulated

the growth of Zn-limited cells (Sunda and Huntsman 1995; Haas et al. 2009; Kellogg et al. 2020). Rather, the growth response of *C. neogracile* RS19 is similar to that observed previously in the substitution-incapable species *C. calcitrans* (Timmermans et al. 2001).

In the analysis of metal: P ratios in C. neogracile RS19, only small variations in Fe: P, Mn: P, Ni: P, Cu: P, Zn: P, and Cd: P quotas across all Co amendments were observed (Fig. 2), reflecting the relatively consistent growth rates attained across these treatments (Fig. 1). Notably, Co: P quotas (and Co uptake rates; Fig. S4b; Table S3) markedly increased with added Co, demonstrating that Co entered the cell, presumably through divalent cation transporters (Fig. 2b). In general, larger variations in metal quotas were observed across Zn treatments. No trend was apparent for Fe, Ni, and Cu quotas with increasing Zn, though maximum quotas for all three elements were higher among Zn treatments compared to Co treatments (Fig. 2a) reflecting a larger metabolic demand as growth rates increased. Mn, Co, and Cd quotas (and Co and Cd uptake rates for $Zn^{2+} > 1e-12 M$; Fig. S4b; Table S3) shared an inverse relationship with $[Zn^{2+}]$, an effect observed previously in marine diatoms due to the upregulation of transport systems induced by low cellular Zn that can also transport Mn, Co, and Cd (Sunda and Huntsman 1996, 1998b, 2000; Hawco and Saito 2018).

Overall, although *C. neogracile* RS19 is incapable of nutritionally substituting Co for Zn, Co uptake still increased with both increasing Co²⁺ and decreasing Zn²⁺ concentrations. The inability to substitute Co is therefore not occurring at the level of import transporters as these quota measurements demonstrate entry of Co into the cell.

The proteomic results, coupled with the physiology and metal quota data, offer the potential to explore the potential

cause(s) for the lack of Zn/Co substitution in *Chaeotoceros*. The Zn metalloproteome can be extraordinarily complex given the many functions Zn has within cellular biochemistry (Mazzotta et al. 2021). In the present study, trends in various Zn metalloproteins were observed that demonstrate active responses to external Zn abundance, implying a complex systems biology with respect to Zn. Below we discuss the transporters, chaperone, and CA responses to varying Zn. While these observations connect Zn availability to specific cellular responses (or lack thereof) and can contribute to hypotheses as to the cause of the lack of Co substitution, we caution that correlations with Zn do not necessarily imply causation and that biochemical characterization on those specific proteins will likely be needed to definitively identify where Co fails to substitute.

The C. neogracile RS19 proteomes generated in the present study revealed distinct responses to Zn vs. Co nutrition. With increasing Co²⁺, maximum spectral counts of both Ch ZIP1 and Ch ZIP2 were observed at the highest added Co²⁺ concentration (17 and 9 spectral counts, respectively; $[Co^{2+}] = 23.47$ pM; Fig. 3e; Table S6), but we found no significant difference comparing spectral counts between low vs. high Co treatments. Increasing [Co²⁺] therefore did not significantly impact the abundance level of either transporter. In contrast, the distinct peaks observed in spectral counts of these ZIP proteins with Zn²⁺ addition is indicative of an acute responsiveness to Zn²⁺ over 0.17–1.1 pM (Fig. 3e). Diatoms are known to possess a high-affinity Zn transport system that is upregulated at free Zn²⁺ concentrations at or above 0.1 nM, but the identity of this transporter was unknown (Sunda and Huntsman 1992, 1998b, 2000). The ZIP transporters detected in C. neogracile are thus likely components of the high-affinity Zn transport system. As the high-affinity Zn uptake system is thought to be nonspecific enough to bind and transport cobalt and cadmium ions (Sunda and Huntsman 1995, 1998b), and ZIP transporters are known to transport multiple metal cations including Fe, Zn, Mn, Co, Cu, and Cd (Guerinot 2000; Brembu et al. 2011; Blaby-Haas and Merchant 2012; Milner et al. 2013), it is likely that the Ch ZIP1 and Ch ZIP2 proteins detected in all Co treatments (Fig. 3e) contributed to the uptake of dCo (Figs. 2b, S4b). While we concluded that Co was not excluded from the cell at the transporter level (Fig. 6), it is also apparent that the ZIP transporters are regulated by Zn availability but not Co availability. Notably, the recently characterized diatom ZCRP-B membrane protein that is thought to be involved in Zn high-affinity transport and is responsive to both Zn and Co was absent in the C. neogracile RS19 proteomes generated in this study (Kellogg et al. 2022).

In addition to the identified ZIP transporters, we also investigated the proteomes of *C. neogracile* RS19 generated in the current Zn/Co study for the presence of membrane transporter families implicated in metal homeostasis in algae. These include the CDFs, P1B-type ATPases, and VIT1 families, all of

which include protein members reportedly involved in algal metal transport (Cobbett et al. 2003; Hanikenne et al. 2005; Blaby-Haas and Merchant 2012; Ibuot et al. 2020). Representative CDF proteins and VIT1 were investigated but were not detected.

P-type ATPases are membrane-bound protein pumps that can transport both monovalent and divalent metal ions (Solioz and Vulpe 1996). ATPase5-1B is a P-type ATPase previously identified in the diatom P. tricornutum that has been implicated in cellular efflux of Cd²⁺ and which shares high similarity to the Cd/Zn transporter HMA4 from the plant genus Arabidopsis (Hanikenne et al. 2008; Brembu et al. 2011; Ma et al. 2020). The C. neogracile RS19 protein P-ATPase1 was identified as a putative P-ATPase based on BLAST similarity to the ATPase5-1B protein in *P. tricornutum* (Fig. S2b; Table S6). P-ATPase1 spectral counts showed an overall decreasing trend with increasing [Co²⁺], with spectral counts ranging from zero (undetected) at the two lowest Zn²⁺ treatments to a maximum of 8 at $[Zn^{2+}] = 3.14 \text{ pM}$ (Fig. 3f). We note that over the range of increasing [Zn²⁺], P-ATPase1 spectral counts increased and Zn quotas increased (Figs. 2a, 3f). We therefore speculate that P-ATPase1 may be acting as a Zn²⁺ efflux transporter in C. neogracile RS19 to balance Zn quotas as growth rates increase, though further characterization is needed.

We next examined the metal chaperones in C. neogracile RS19. Recently we characterized ZCRP-A as an intracellular protein with a conserved Zn²⁺-binding domain that is thought to act as a metal chaperone in Zn/Co-limited diatoms based on the inverse relationship between ZCRP-A abundance and Zn²⁺ and Co²⁺ media concentrations in the marine diatoms T. pseudonana CCMP1335, P. tricornutum CCMP632, and P. delicatissima UNC1205 (Kellogg et al. 2022). In the present study, ZCRP-A increased in abundance in proteomes generated under low [Zn²⁺] (Fig. 3g) in C. neogracile RS19 double addition experiments. Total ZCRP-A spectral counts were not modulated by increasing [Co²⁺], but instead responded to the background amount of 1.1 pM Zn and the specific growth rate achieved in these treatments (Fig. 3g). Indeed, ZCRP-A spectral counts and specific growth rates over all double addition treatments shared a significant negative linear relationship (twoway linear regression, $R^2 = 0.67$, p = 0.02; Fig. S3c), similar to that observed previously in the diatom P. tricornutum (Kellogg et al. 2022). The positive linear relationship between ZIP proteins and ZCRP-A ($R^2 = 0.58$, p = 0.05; Fig. S3d) in C. neogracile RS19 furthermore suggested that ZCRP-A may be controlled by a shared sensor and regulator system, and is likely critical to Zn homeostasis in this organism by serving as a Zn chaperone (as characterized in Kellogg et al. 2022). This effect of [Zn²⁺] on ZCRP-A expression patterns agrees with our previous findings in C. neogracile RS19, yet implies this protein is responsive only to Zn in this particular diatom. Importantly, the ZCRP-A protein in C. neogracile RS19 is unique among other diatom homologs as it lacks the conserved G2/Switch I region, which negates the predicted Zn²⁺-binding site (Kellogg et al. 2022) and which we hypothesize may contribute to this behavior. Further work is required to investigate the metal-binding capability of ZCRP-A in this diatom, though it is notable that the expression of this protein in C. neogracile RS19 was not significantly modulated by increasing [Co²⁺].

We next considered the metal-binding domains in the CAs of *C. neogracile* RS19, with a specific focus on whether known CA active site domains and structures can accommodate Co, and if this substitution would affect enzymatic efficiency. As the restoration of Zn-limited growth by addition of Co in diatoms has long been hypothesized to be conferred by the interreplacement of these metals in CAs, we explored the classes of these CAs present and expression patterns in response to Zn and Co in *C. neogracile* RS19. *C. neogracile* expressed putative α , γ , and θ -CAs in response to our Zn and Co addition experiments (Fig. 3c,d). Four of the six detected CAs (α -CA, θ -CA1, θ -CA2, and θ -CA3) increased in abundance with increasing [Zn²⁺], but not with increasing [Co²⁺], while abundances of γ -CA and θ -CA4 did not significantly change over all metal treatments (Fig. 3c,d).

Biochemical studies of the α -CA class have mainly been performed on human carbonic anhydrase II, which is known to bind Zn²⁺ at the active site tetrahedrally coordinated by three histidine residues and a water or hydroxide molecule (Liljas et al. 1972; Håkansson et al. 1992). While in vitro substitution of Co²⁺ at the active site of bovine carbonic anhydrase II has been documented, the Co-containing form results in decreased enzyme activity compared to the native Zn form (Tu and Silverman 1985). The α -CA detected in C. neogracile had highest similarity to P. tricornutum CA-III. Tachibana et al. (2011) have previously characterized CA-III as an α -CA that localizes to the chloroplast endoplasmic reticulum. While the predicted active site of P. tricornutum CA-III does not possess the three His residues known to form a Zn²⁺ coordination site (Tachibana et al. 2011), we note that C. neogracile α -CA possesses all three His residues (Fig. S1a). Based on these conserved Zn²⁺ coordination residues, it is possible that Co^{2+} can also be coordinated in C. neogracile α -CA, and the effects on activity could be examined in future studies.

Carbonic anhydrase methanosarcina (CAM), the prototype of the γ -CA class isolated from the methanogenic archaeon *Methanosarcina thermophila*, is the only γ -CA crystallized to date and is known to use a Zn²⁺ cofactor that can be replaced by Co²⁺ and Fe²⁺ (Iverson et al. 2000; Innocenti et al. 2004; MacAuley et al. 2009; Ferry 2010; Supuran and Capasso 2017). The ability of γ -CAs to replace Zn²⁺ with either of these metals has not yet been observed in photosynthetic organisms, and it is unclear if γ -CAs are involved in the CCM (DiMario et al. 2017). *C. neogracile* γ -CA had high sequence similarity to both *T. pseudonana* CA-13 and *P. tricomutum* CA-VIII, both of which are mitochondrial γ -CAs (Fig. S1b; Table S5) (Tachibana et al. 2011; Samukawa et al. 2014). A recent study has shown that diatom γ -CA is part of mitochondrial complex I, though

it is unknown if the role of γ -CA is purely structural or if it is capable of converting bicarbonate into CO_2 (Cainzos et al. 2021). Like CA-13 and CA-VIII, the predicted active site of *C. neogracile* γ -CA possesses only two of the three conserved His residues seen in CAM (Fig. S1b). However, γ -CA possesses the potential Zn ligands His, Cys, or Asp near the putative Zn coordination site and thus may retain activity with Zn²⁺.

The first member of the θ -CA class, Pt43233, was recently discovered in P. tricornutum. Pt43233 localizes to the thylakoid lumen, contains a well-conserved sequence forming a putative divalent cation-chelating moiety, and is suggested to play a role in both photosynthesis and the CCM (Kikutani et al. 2016). While BLAST analysis has demonstrated the presence of θ -CAs in other diatoms (Jensen et al. 2020), there are as of yet no studies investigating enzyme activity or efficiency with Co^{2+} . With the exception of θ -CA4, the predicted active sites of C. neogracile θ -CAs possess only two or three of the four putative Zn coordination residues seen in Pt43233 (Fig. S1c), but like the γ -CAs, possess His, Cys, or Asp that may contribute to the Zn coordination site. Further research into divalent metal coordination at the active site of diatom CAs would elucidate the possibility of Co²⁺ exclusion at the level of α , γ , and θ -CAs in *C. neogracile* RS19.

The different cellular localizations of these CAs further complicates our consideration of where Co^{2+} exclusion is occurring. In this study, we describe CAs in *C. neogracile* RS19 with high sequence similarity to CAs that have been shown to localize to the chloroplast endoplasmic reticulum, the mitochondria, and the thylakoid lumen (Table S5). CAs within these organelles must necessarily acquire their metal cofactors via a system of transporters and chaperones, which may or may not be metal selective, that deliver them through membranes. CA localization is thus another factor that may influence Zn/Co metabolic substitution in diatoms.

We did not detect homologs of the known Co/Zn-binding δ -CA (also called TWCA1 for *T. weissflogii* carbonic anhydrase), the Cd/Zn-binding ζ -CA (also called CDCA1 for Cd carbonic anhydrase), nor the Mn/Zn-binding ι -CA that have been previously described in diatoms (Jensen et al. 2019; Lane and Morel 2000a). It is important to note that, since the raw protein spectra in this study were matched to proteins using a transcriptome rather than a complete genome as a database as no complete genome is available at this time (see methods), additional CAs in *C. neogracile* RS19 may exist. However, we find it notable that we detected no others in this Zn/Co limitation study beyond the α -CA, γ -CA, and θ -CAs reported here, and note that any other abundantly expressed CAs should have been detected in the proteomic analysis using the transcriptome database.

In the present study, the combination of metal quota data, protein expression patterns, and classes of CAs present in *C. neogracile* RS19 imply that Co exclusion is occurring intracellularly at the metalloprotein level rather than by exclusion via transporter selectivity. There are several known Zn

metalloproteins present in the proteome that could be the site where Zn/Co cambialism is failing in this diatom. First, the restoration of Zn-limited growth by addition of Co (and Cd) in diatoms has been previously attributed to CAs, based on observations of metal interreplacement within in vivo radio-labeling studies (Yee and Morel 1996) and immunological assays of protein expression (Lane and Morel 2000*b*).

It is possible that the CAs detected in this diatom during Zn/Co limitation are more catalytically efficient with Zn²⁺, which could result in the inability to recover the growth rate of C. neogracile with low Zn and added Co in the double addition experiments, as some cambialistic diatom CAs have reduced efficiency with alternate metals such as Co or Cd (Xu et al. 2008). The specific growth rates obtained in double addition experiments with increasing Zn²⁺ and constant Co²⁺ (Fig. 2b) were not significantly different compared to those obtained in simple Zn²⁺ addition with no additional Co²⁺ (paired t-test; p = 0.79; Fig. 2a), implying no additive benefit of Co with Zn, and hence no physiological evidence of cambialism. A significant positive relationship was observed between specific growth rate and CA abundance (Fig. S3e) and was consistent with prior observations of reduced CA activity under Zn-limited growth (McGinn and Morel 2008). Yet, we did not observe a significant relationship between cellular Zn quotas and CA abundance, implying that CAs were not dominating the cellular Zn reservoir at the low Zn range (Fig. S3f). Together these results imply that growth rates influenced CA abundance, consistent with the greater photosynthetic demand for carbon and need for CA at higher growth rates.

We further note that at the two lowest added Zn^{2+} concentrations in double addition experiments, no CAs of any type were detected using global data dependent analysis despite a background concentration of 2.37 pM Co^{2+} , although more sensitive targeted methods could be employed in the future (Fig. 3c,d). While we did not explore the ability of this diatom to substitute Cd^{2+} in place of Zn^{2+} , we did not detect any CAs in this diatom's CA portfolio with significant BLAST similarity to the Cd-binding ζ -CA, CDCA1. Together, the lack of the well-characterized cambialistic diatom CAs in RS19 (δ -CA and ζ -CA), and the decreased abundance of CAs at low Zn^{2+} concentrations implies that CAs were likely not solely responsible for the lack of Co substitution in this diatom, nor were they solely responsible for the decrease in specific growth rate at low Zn^{2+} concentrations.

Other Zn-requiring proteins were also detected in the proteome, notably RNA polymerase and Zn finger proteins. These proteins are involved in transcription and translation and were observed to increase within increasing Zn (Fig. 3a,b), and had significant positive relationships with specific growth rate (Fig. S3a,b). This RNA polymerase correlation is promising with regards to interest in developing molecular proxies for growth rate, and is consistent with prior observations of decreased ribosomal proteins under phosphorus deficiency in the diatom *T. pseudonana* (Dyhrman et al. 2012). Future

studies could examine if there is a robust relationship with other limiting nutrients that could be further developed. Zn finger proteins are often thought to be very low copy number proteins, and hence it was surprising for them to be detectable and show correlations with Zn in the present study. While both RNA polymerase and Zn finger proteins are generally considered Zn-requiring proteins, Co substitution has been reported in vivo for RNA polymerase (Speckhard et al. 1977) and has been found to cause toxicity (Predki and Sarkar 1994). As with the CAs, biochemical studies with diatom proteins are needed to identify the potential mechanisms giving rise to an (in)ability to substitute Co for Zn.

Conclusions

The ability to use Co to restore Zn-limited growth rates in diatoms is clearly species-specific, with C. calcitrans, C. simplex, and now C. neogracile RS19 shown to be incapable of substituting Co in place of Zn. Although there are likely other marine algae that lack the Zn/Co substitution ability, it is notable that the only three diatoms found to lack this ability thus far are members of the genus Chaetoceros. In this study, transporters, chaperones, RNA polymerases, Zn finger proteins, and certain CAs all showed relationships to Zn and/or growth rate. While quota data demonstrates that Co enters the cell, it is unable to substitute for Zn to allow the cell to recover physiologically under low Zn. Given that many of the proteins described above respond to Zn but not Co, we speculate that the inability to Zn/Co substitute is occurring at the enzyme level in C. neogracile RS19. To our knowledge, little is known about what proteins are involved in intracellular Zn sensing and homeostasis in marine diatoms. As the only CAs detected in C. neogracile in this study belonged to the α , γ , and θ classes, all of which are not known to retain maximal activity with a Co cofactor, the lack of Zn/Co cambialistic CAs in this diatom could also contribute to the observed growth trends.

As Zn/Co substitution is hypothesized to confer a competitive advantage to substitution-capable phytoplankton species when faced with extremely low concentrations of bioavailable Zn, this species-specific ability should influence community composition. The responsiveness of different diatom species to Zn and Co may affect their competitiveness within the algal community, leading to spatial and temporal differences in species-specific primary production. We hypothesize that oceanic environments high in Zn may select for substitutionincapable diatom strains, as these diatoms would likely be at a growth disadvantage compared to substitution-capable diatoms in Zn-limited environments. For example, we have previously demonstrated that diatoms isolated from the northeast Pacific, where relatively high surface dCo: dZn ratios were observed, had enhanced abilities to use Co to relieve Znlimited growth rates in culture (Kellogg et al. 2020). The surface northeast Pacific is therefore an example of a low dZn,

high dCo region that hosts substitution-capable diatoms. In contrast, C. neogracile RS19 was isolated from the Ross Sea of Antarctica, which is an example of a high Zn environment. dZn surface concentrations typically range from ~ 3 –5 nM with seasonal drawdowns to ~ 0.5 –2 nM occurring during summer (Fitzwater et al. 2000; Coale et al. 2005). The genus Chaetoceros provides an interesting example of a nonsubstituting diatom, and further biochemical and metalloproteomic characterization will enable a better understanding of the nature of Zn/Co cambialism and its effect on marine community composition.

Data availability statement

The *Chaetoceros neogracile* RS19 mass spectrometry global proteomics dataset generated here and transcriptome-derived FASTA database file used for peptide to spectrum matching (PSMs) generated under replete and iron-limited conditions (see above) were submitted to the ProteomeXchange Consortium through the PRIDE (Perez-Riverol et al. 2019) partner repository with the dataset identifiers PXD026895 and 10. 6019/PXD026895. Growth rate and metal quota data from this analysis have been submitted through the NSF's Biological and Chemical Oceanography Data Management Office (BCO-DMO) repository. Code used to create the volcano plots and heatmap is available on Github (https://github.com/mkell0gg/ChRS19_2021_heatmap_volcanoplot).

References

- Armbrust, E. V., and others. 2004. The genome of the diatom *Thalassiosira pseudonana*: Ecology, evolution, and metabolism. Science **306**: 79–86. doi:10.1126/science.1101156
- Badger, M. 2003. The roles of carbonic anhydrases in photosynthetic CO_2 concentrating mechanisms. Photosynth. Res. **77**: 83. doi:10.1023/A:1025821717773
- Badger, M. R., and G. D. Price. 1994. The role of carbonic anhydrase in photosynthesis. Annu. Rev. Plant. Physiol. Plant. Mol. Biol. **45**: 369–392. doi:10.1146/annurev.pp.45. 060194.002101
- Badger, M. R., T. J. Andrews, S. M. Whitney, M. Ludwig, D. C. Yellowlees, W. Leggat, and G. D. Price. 1998. The diversity and coevolution of Rubisco, plastids, pyrenoids, and chloroplast-based CO₂-concentrating mechanisms in algae. Can. J. Bot. **76**: 1052–1071. doi:10.1139/b98-074
- Blaby-Haas, C. E., and S. S. Merchant. 2012. The ins and outs of algal metal transport. Biochim. Biophys. Acta **1823**: 1531–1552. doi:10.1016/j.bbamcr.2012.04.010
- Bowler, C., and others. 2008. The *Phaeodactylum* genome reveals the evolutionary history of diatom genomes. Nature **456**: 239–244. doi:10.1038/nature07410
- Brembu, T., M. Jørstad, P. Winge, K. C. Valle, and A. M. Bones. 2011. Genome-wide profiling of responses to cadmium in the diatom *Phaeodactylum tricornutum*. Environ. Sci. Technol. **45**: 7640–7647. doi:10.1021/es2002259

- Burkhardt, S., G. Amoroso, U. Riebesell, and D. Sültemeyer. 2001. CO₂ and HCO₃- uptake in marine diatoms acclimated to different CO₂ concentrations. Limnol. Oceanogr. **46**: 1378–1391. doi:10.4319/lo.2001.46.6.1378
- Cainzos, M., F. Marchetti, C. Popovich, P. Leonardi, G. Pagnussat, and E. Zabaleta. 2021. Gamma carbonic anhydrases are subunits of the mitochondrial complex I of diatoms. Mol. Microbiol. **116**: 109–125. doi:10.1111/mmi.14694
- Coale, K. H., R. Michael Gordon, and X. Wang. 2005. The distribution and behavior of dissolved and particulate iron and zinc in the Ross Sea and Antarctic circumpolar current along 170°W. Deep Sea Res. Part I Oceanogr. Res. Pap. **52**: 295–318. doi:10.1016/j.dsr.2004.09.008
- Cobbett, C. S., D. Hussain, and M. J. Haydon. 2003. Structural and functional relationships between type 1_B heavy metal-transporting P-type ATPases in *Arabidopsis*. New Phytol. **159**: 315–321. doi:10.1046/j.1469-8137.2003.00785.x
- DiMario, R. J., H. Clayton, A. Mukherjee, M. Ludwig, and J. V. Moroney. 2017. Plant carbonic anhydrases: Structures, locations, evolution, and physiological roles. Mol. Plant **10**: 30–46. doi:10.1016/j.molp.2016.09.001
- DiMario, R. J., M. C. Machingura, G. L. Waldrop, and J. V. Moroney. 2018. The many types of carbonic anhydrases in photosynthetic organisms. Plant Sci. **268**: 11–17. doi:10. 1016/j.plantsci.2017.12.002
- Dyhrman, S. T., and others. 2012. The transcriptome and proteome of the diatom *Thalassiosira pseudonana* reveal a diverse phosphorus stress response. PLoS One **7**: e33768. doi:10.1371/journal.pone.0033768
- Edgar, R. C. 2004. MUSCLE: Multiple sequence alignment with high accuracy and high throughput. Nucleic Acids Res. **32**: 1792–1797. doi:10.1093/nar/gkh340
- Elzenga, J. T. M., H. B. A. Prins, and J. Stefels. 2000. The role of extracellular carbonic anhydrase activity in inorganic carbon utilization of *Phaeocystis globosa* (Prymnesiophyceae): A comparison with other marine algae using the isotopic disequilibrium technique. Limnol. Oceanogr. **45**: 372–380. doi:10. 4319/lo.2000.45.2.0372
- Espie, G. S., and B. Colman. 2005. CO₂-concentrating mechanisms in aquatic photosynthetic microorganisms. Can. J. Bot. **83**: 695–697. doi:10.1139/b05-907
- Ferry, J. G. 2010. The γ class of carbonic anhydrases. Biochim. Biophys. Acta **1804**: 374–381. doi:10.1016/j.bbapap.2009. 08.026
- Fitzwater, S. E., K. S. Johnson, R. M. Gordon, K. H. Coale, and W. O. Smith. 2000. Trace metal concentrations in the Ross Sea and their relationship with nutrients and phytoplankton growth. Deep Sea Res. Part II Top. Stud. Oceanogr. **47**: 3159–3179. doi:10.1016/S0967-0645(00)00063-1
- Glover, D. M., W. J. Jenkins, and S. C. Doney. 2011. Modeling methods for marine science. Cambridge Univ. Press.
- Guerinot, M. L. 2000. The ZIP family of metal transporters. Biochim. Biophys. Acta **1465**: 190–198. doi:10.1016/S0005-2736(00)00138-3

- Haas, C. E., D. A. Rodionov, J. Kropat, D. Malasarn, S. S. Merchant, and V. de Crécy-Lagard. 2009. A subset of the diverse COG0523 family of putative metal chaperones is linked to zinc homeostasis in all kingdoms of life. BMC Genomics 10: 470. doi:10.1186/1471-2164-10-470
- Håkansson, K., M. Carlsson, L. A. Svensson, and A. Liljas. 1992. Structure of native and apo carbonic anhydrase II and structure of some of its anion-ligand complexes. J. Mol. Biol. **227**: 1192–1204. doi:10.1016/0022-2836(92)90531-N
- Hanikenne, M., U. Krämer, V. Demoulin, and D. Baurain. 2005. A comparative inventory of metal transporters in the green alga *Chlamydomonas reinhardtii* and the red alga *Cyanidioschizon merolae*. Plant Physiol. **137**: 428–446. doi: 10.1104/pp.104.054189
- Hanikenne, M., and others. 2008. Evolution of metal hyperaccumulation required *cis*-regulatory changes and triplication of *HMA4*. Nature **453**: 391–395. doi:10.1038/nature06877
- Hawco, N. J., and M. A. Saito. 2018. Competitive inhibition of cobalt uptake by zinc and manganese in a pacific *Prochlorococcus* strain: Insights into metal homeostasis in a streamlined oligotrophic cyanobacterium. Limnol. Oceanogr. 63: 2229–2249. doi:10.1002/lno.10935
- Hewett-Emmett, D., and R. E. Tashian. 1996. Functional diversity, conservation, and convergence in the evolution of the α -, β -, and γ -carbonic anhydrase gene families. Mol. Phylogenet. Evol. **5**: 50–77. doi:10.1006/mpev.1996.0006
- Hopkinson, B. M., C. Meile, and C. Shen. 2013. Quantification of extracellular carbonic anhydrase activity in two marine diatoms and investigation of its role. Plant Physiol. **162**: 1142–1152. doi:10.1104/pp.113.217737
- Hughes, C. S., S. Foehr, D. A. Garfield, E. E. Furlong, L. M. Steinmetz, and J. Krijgsveld. 2014. Ultrasensitive proteome analysis using paramagnetic bead technology. Mol. Syst. Biol. **10**: 757. doi:10.15252/msb.20145625
- Ibuot, A., A. P. Dean, and J. K. Pittman. 2020. Multi-genomic analysis of the cation diffusion facilitator transporters from algae. Metallomics **12**: 617–630. doi:10.1039/D0MT00009D
- Innocenti, A., S. Zimmerman, J. Ferry, A. Scozzafava, and C. Supuran. 2004. Carbonic anhydrase inhibitors. Inhibition of the beta-class enzyme from the methanoarchaeon *Methanobacterium thermoautotrophicum* (Cab) with anions. Bioorg. Med. Chem. Lett. **14**: 4563–4567. doi:10.1016/j. bmcl.2004.06.073
- Iverson, T. M., B. E. Alber, C. Kisker, J. G. Ferry, and D. C. Rees. 2000. A closer look at the active site of γ -class carbonic anhydrases: High-resolution crystallographic studies of the carbonic anhydrase from *Methanosarcina thermophila*. Biochemistry **39**: 9222–9231. doi:10.1021/bi000204s
- Jensen, E. L., R. Clement, A. Kosta, S. C. Maberly, and B. Gontero. 2019. A new widespread subclass of carbonic anhydrase in marine phytoplankton. ISME J. **13**: 2094–2106. doi:10.1038/s41396-019-0426-8

- Jensen, E. L., S. C. Maberly, and B. Gontero. 2020. Insights on the functions and ecophysiological relevance of the diverse carbonic anhydrases in microalgae. Int. J. Mol. Sci. **21**: 2922. doi:10.3390/ijms21082922
- Kang, S. H., J. S. Kang, S. Lee, K. H. Chung, D. Kim, and M. G. Park. 2001. Antarctic phytoplankton assemblages in the marginal ice zone of the northwestern Weddell Sea. J. Plankton Res. 23: 333–352. doi:10.1093/plankt/23.4.333
- Keller, M. D., W. K. Bellows, and R. R. L. Guillard. 1988. Microwave treatment for sterilization of phytoplankton culture media. J. Exp. Mar. Bio. Ecol. 117: 279–283. doi:10. 1016/0022-0981(88)90063-9
- Kellogg, R. M., M. R. McIlvin, J. Vedamati, B. S. Twining, J. W. Moffett, A. Marchetti, D. M. Moran, and M. A. Saito. 2020. Efficient zinc/cobalt inter-replacement in northeast Pacific diatoms and relationship to high surface dissolved Co:Zn ratios. Limnol. Oceanogr. 65: 2557–2582. doi:10.1002/lno.11471
- Kellogg, R. M., and others. 2022. Adaptive responses of marine diatoms to zinc scarcity and ecological implications. Nat. Commun. **13**: 1995. doi:10.1038/s41467-022-29603-y
- Kikutani, S., K. Nakajima, C. Nagasato, Y. Tsuji, A. Miyatake, and Y. Matsuda. 2016. Thylakoid luminal θ-carbonic anhydrase critical for growth and photosynthesis in the marine diatom *Phaeodactylum tricornutum*. Proc. Natl. Acad. Sci. USA **113**: 9828–9833. doi:10.1073/pnas.1603112113
- Koch, F., and S. Trimborn. 2019. Limitation by Fe, Zn, Co, and B_{12} results in similar physiological responses in two antarctic phytoplankton species. Front. Mar. Sci. **6**: 514. doi:10. 3389/fmars.2019.00514
- Krishna, S. S. 2003. Structural classification of zinc fingers: Survey and summary. Nucleic Acids Res. **31**: 532–550. doi:10. 1093/nar/gkg161
- Krogh, A., B. Larsson, G. von Heijne, and E. L. L. Sonnhammer. 2001. Predicting transmembrane protein topology with a hidden Markov model: Application to complete genomes. J. Mol. Biol. **305**: 567–580. doi:10. 1006/jmbi.2000.4315
- Kumar, S., G. Stecher, M. Li, C. Knyaz, and K. Tamura. 2018. MEGA X: Molecular Evolutionary Genetics Analysis across computing platforms. Mol. Biol. Evol. 35: 1547–1549. doi: 10.1093/molbev/msy096
- Lane, T. W., and F. M. Morel. 2000*a*. A biological function for cadmium in marine diatoms. Proc. Natl. Acad. Sci. USA **97**: 4627–4631. doi:10.1073/pnas.090091397
- Lane, T. W., and F. M. M. Morel. 2000*b*. Regulation of carbonic anhydrase expression by zinc, cobalt, and carbon dioxide in the marine diatom *Thalassiosira weissflogii*. Plant Physiol. **123**: 345–352. doi:10.1104/pp.123.1.345
- Lane, T. W., M. A. Saito, G. N. George, I. J. Pickering, R. C. Prince, and F. M. M. Morel. 2005. A cadmium enzyme from a marine diatom. Nature **435**: 42. doi:10.1038/435042a
- Lasbleiz, M., K. Leblanc, L. K. Armand, U. Christaki, C. Georges, I. Obernosterer, and B. Quéguiner. 2016.

- Composition of diatom communities and their contribution to plankton biomass in the naturally iron-fertilized region of Kerguelen in the Southern Ocean. FEMS Microbiol. Ecol. **92**: fiw171. doi:10.1093/femsec/fiw171
- Lee, J., and F. Morel. 1995. Replacement of zinc by cadmium in marine phytoplankton. Mar. Ecol. Prog. Ser. **127**: 305–309. doi:10.3354/meps127305
- Leventer, A. 1991. Sediment trap diatom assemblages from the northern Antarctic Peninsula region. Deep Sea Res. Part I Oceanogr. Res. Pap. **38**: 1127–1143. doi:10.1016/0198-0149(91)90099-2
- Liljas, A., and others. 1972. Crystal structure of human carbonic anhydrase C. Nat. New Biol. **235**: 131–137. doi:10. 1038/newbio235131a0
- Ma, J., B. Zhou, Q. Tan, L. Zhang, and K. Pan. 2020. The roles of silicon in combating cadmium challenge in the marine diatom *Phaeodactylum tricomutum*. J. Hazard. Mater. **389**: 121903. doi:10.1016/j.jhazmat.2019.121903
- MacAuley, S. R., S. A. Zimmerman, E. E. Apolinario, C. Evilia, Y.-M. Hou, J. G. Ferry, and K. R. Sowers. 2009. The archetype γ -class carbonic anhydrase (Cam) contains iron when synthesized in vivo. Biochemistry **48**: 817–819. doi:10. 1021/bi802246s
- Mazzotta, M. G., M. R. McIlvin, D. M. Moran, D. T. Wang, K. D. Bidle, C. H. Lamborg, and M. A. Saito. 2021. Characterization of the metalloproteome of *Pseudoalteromonas* (BB2-AT2): Biogeochemical underpinnings for zinc, manganese, cobalt, and nickel cycling in a ubiquitous marine heterotroph. Metallomics 13: mfab060. doi:10.1093/mtomcs/mfab060
- McGinn, P. J., and F. M. M. Morel. 2008. Expression and regulation of carbonic anhydrases in the marine diatom *Thalassiosira pseudonana* and in natural phytoplankton assemblages from Great Bay, New Jersey. Physiol. Plant. **133**: 78–91. doi:10.1111/j.1399-3054.2007.01039.x
- Milner, M. J., J. Seamon, E. Craft, and L. V. Kochian. 2013. Transport properties of members of the ZIP family in plants and their role in Zn and Mn homeostasis. J. Exp. Bot. **64**: 369–381. doi:10.1093/jxb/ers315
- Morel, F. M. M., P. J. Lam, and M. A. Saito. 2020. Trace metal substitution in marine phytoplankton. Annu. Rev. Earth Planet. Sci. **48**: 491–517. doi:10.1146/annurev-earth-053018-060108
- Moroney, J. V., H. D. Husic, and N. E. Tolbert. 1985. Effect of carbonic anhydrase inhibitors on inorganic carbon accumulation by *Chlamydomonas reinhardtii*. Plant Physiol. **79**: 177–183. doi:10.1104/pp.79.1.177
- Perez-Riverol, Y., and others. 2019. The PRIDE database and related tools and resources in 2019: Improving support for quantification data. Nucleic Acids Res. **47**: 442–450. doi:10. 1093/nar/gky1106
- Predki, P. F., and B. Sarkar. 1994. Metal replacement in "zinc finger" and its effect on DNA binding. Environ. Health Perspect. **102**: 195–198. doi:10.1289/ehp.94102s3195

- Price, N. M., and F. M. M. Morel. 1990. Cadmium and cobaltsubstitution for zinc in a marine diatom. Nature **344**: 658–660. doi:10.1038/344658a0
- Saito, M. A., and T. J. Goepfert. 2008. Zinc-cobalt colimitation of *Phaeocystis antarctica*. Limnol. Oceanogr. **53**: 266–275. doi:10.4319/lo.2008.53.1.0266
- Saito, M. A., V. V. Bulygin, D. M. Moran, C. Taylor, and C. Scholin. 2011. Examination of microbial proteome preservation techniques applicable to autonomous environmental sample collection. Front. Microbiol. 2: 215. doi:10.3389/fmicb.2011.00215
- Samukawa, M., C. Shen, B. M. Hopkinson, and Y. Matsuda. 2014. Localization of putative carbonic anhydrases in the marine diatom, *Thalassiosira pseudonana*. Photosynth. Res. **121**: 235–249. doi:10.1007/s11120-014-9967-x
- So, A. K.-C., G. S. Espie, E. B. Williams, J. M. Shively, S. Heinhorst, and G. C. Cannon. 2004. A novel evolutionary lineage of carbonic anhydrase (epsilon class) is a component of the carboxysome shell. J. Bacteriol. **186**: 623–630. doi:10.1128/JB.186.3.623-630.2004
- Solioz, M., and C. Vulpe. 1996. CPx-type ATPases: A class of P-type ATPases that pump heavy metals. Trends Biochem. Sci. 21: 237–241. doi:10.1016/S0968-0004(96)20016-7
- Speckhard, D. C., F. Y. H. Wu, and C.-W. Wu. 1977. Role of the intrinsic metal in RNA polymerase from *Escherichia coli*. In vivo substitution of tightly bound zinc with cobalt. Biochemistry **16**: 5228–5234. doi:10.1021/bi00643a011
- Sunda, W. G., and S. A. Huntsman. 1992. Feedback interactions between zinc and phytoplankton in seawater. Limnol. Oceanogr. **37**: 25–40. doi:10.4319/lo.1992.37.1.0025
- Sunda, W. G., and S. A. Huntsman. 1995. Cobalt and zinc interreplacement in marine phytoplankton: Biological and geochemical implications. Limnol. Oceanogr. **40**: 1404–1417. doi:10.4319/lo.1995.40.8.1404
- Sunda, W. G., and S. A. Huntsman. 1996. Antagonisms between cadmium and zinc toxicity and manganese limitation in a coastal diatom. Limnol. Oceanogr. **41**: 373–387. doi:10.4319/lo.1996.41.3.0373
- Sunda, W. G., and S. A. Huntsman. 1998*a*. Interactions among Cu^{2+} , Zn^{2+} , and Mn^{2+} in controlling cellular Mn, Zn, and growth rate in the coastal alga *Chlamydomonas*. Limnol. Oceanogr. **43**: 1055–1064. doi:10.4319/lo.1998.43.6.1055
- Sunda, W. G., and S. A. Huntsman. 1998*b*. Control of Cd concentrations in a coastal diatom by interactions among free ionic Cd, Zn, and Mn in seawater. Environ. Sci. Technol. **32**: 2961–2968. doi:10.1021/es980271y
- Sunda, W. G., and S. A. Huntsman. 2000. Effect of Zn, Mn, and Fe on Cd accumulation in phytoplankton: Implications for oceanic Cd cycling. Limnol. Oceanogr. **45**: 1501–1516. doi:10.4319/lo.2000.45.7.1501
- Sunda, W. G., and S. A. Huntsman. 2005. Effect of CO_2 supply and demand on zinc uptake and growth limitation in a coastal diatom. Limnol. Oceanogr. **50**: 1181–1192. doi:10. 4319/lo.2005.50.4.1181

- Sunda, W. G., N. M. Price, and F. M. M. Morel. 2005. Trace metal ion buffers and their use in culture studies, p. 35–63. *In* Algal culturing techniques. Elsevier.
- Supuran, C., and C. Capasso. 2017. An overview of the bacterial carbonic anhydrases. Metabolites **7**: 56. doi:10.3390/metabo7040056
- Tachibana, M., A. E. Allen, S. Kikutani, Y. Endo, C. Bowler, and Y. Matsuda. 2011. Localization of putative carbonic anhydrases in two marine diatoms, *Phaeodactylum tricornutum* and *Thalassiosira pseudonana*. Photosynth. Res. **109**: 205–221. doi:10.1007/s11120-011-9634-4
- Timmermans, K. R., J. Snoek, L. J. A. Gerringa, I. Zondervan, and H. J. W. de Baar. 2001. Not all eukaryotic algae can replace zinc with cobalt: *Chaetoceros calcitrans* (Bacillariophyceae) versus *Emiliania huxleyi* (Prymnesiophyceae). Limnol. Oceanogr. **46**: 699–703. doi:10.4319/lo.2001.46.3.0699
- Tu, C. K., and D. N. Silverman. 1985. Catalysis by cobalt(II)-substituted carbonic anhydrase II of the exchange of oxygen-18 between $\rm CO_2$ and $\rm H_2O$. Biochemistry **24**: 5881–5887. doi: $10.1021/\rm bi00342a029$
- Xu, Y., D. Tang, Y. Shaked, and F. M. M. Morel. 2007. Zinc, cadmium, and cobalt interreplacement and relative use efficiencies in the coccolithophore *Emiliania huxleyi*. Limnol. Oceanogr. **52**: 2294–2305. doi:10.4319/lo.2007. 52.5.2294
- Xu, Y., L. Feng, P. D. Jeffrey, Y. Shi, and F. M. M. Morel. 2008. Structure and metal exchange in the cadmium carbonic

- anhydrase of marine diatoms. Nature **452**: 56–61. doi:10. 1038/NATURE06636
- Yee, D., and F. M. M. Morel. 1996. In vivo substitution of zinc by cobalt in carbonic anhydrase of a marine diatom. Limnol. Oceanogr. **41**: 573–577. doi:10.4319/lo.1996.41.3. 0573
- Zhang, Y., Z. Wen, M. P. Washburn, and L. Florens. 2010. Refinements to label free proteome quantitation: How to deal with peptides shared by multiple proteins. Anal. Chem. **82**: 2272–2281. doi:10.1021/ac9023999

Acknowledgments

We thank Deepa Rao for assistance with python and R coding. We also thank Caitlyn Kelleher and four anonymous reviewers for feedback on an earlier draft. This work was funded by National Science Foundation (NSF) awards 2123055, 2125063, 1643684, 1850719, and 1924554, and by National Institutes of Health (NIH) award GM135709-01A1. RMK was supported by the Stanley Watson Foundation.

Conflict of Interest

None declared.

Submitted 25 June 2021 Revised 14 December 2021 Accepted 19 July 2022

Associate editor: C. Elisa Schaum